Impacts of Sea Ice Leads on Sea Salt Aerosols and Atmospheric Chemistry in the Arctic

Erin J. Emme[1,*]; Hannah M. Horowitz[1,2,*]

[1]Department of Civil and Environmental Engineering, University of Illinois Urbana-Champaign, Urbana, Illinois, USA

[2]Department of Atmospheric Science, University of Illinois Urbana-Champaign, Urbana, Illinois, USA

For submission to

Atmospheric Chemistry and Physics

February 6, 2025

---

*Corresponding authors: Erin J. Emme, emme2@illinois.edu, and Hannah M. Horowitz, hmhorow@illinois.edu.

Impacts of Sea Ice Leads on Sea Salt Aerosols and Atmospheric Chemistry in the Arctic

Erin J. Emme[1], Hannah M. Horowitz[1,2]

[1]Department of Civil and Environmental Engineering, University of Illinois at Urbana-Champaign, Urbana, 61801, USA

[2]Department of Atmospheric Sciences, University of Illinois at Urbana-Champaign, Urbana, 61801, USA

***Correspondence to*: Erin J. Emme (emme@illinois.edu) and Hannah Horowitz (hmhorow@illinois.edu)**

Abstract. The processes contributing to Arctic cold season (November-April) sea salt aerosols (SSA) remain uncertain. Observations from coastal Alaska suggest emissions from open leads in sea ice, which are not included in climate models, may play a dominant role. Their Arctic-wide significance has not yet been quantified. Here, we create an emissions parameterization of SSA from leads by combining satellite data of lead area (the AMSR-E product) and a chemical transport model (GEOS-Chem) to quantify pan-Arctic SSA emissions from leads during the cold season from 2002-2008 and predict their impacts on atmospheric chemistry, evaluating the results of our simulated SSA against in-situ observations. The AMSR-E product detects large leads with certainty (>3 km in size) and hence our study is limited to quantifying emissions from large leads. Lead emissions vary seasonally and interannually. Simulated total monthly SSA emissions increase by 1.1-1.8% (≥60°N latitude) and 5.6-7.5% (≥75°N) for the 2002-2008 cold season. SSA concentrations increase primarily at the location of leads, where standard model concentrations are low. GEOS-Chem overestimates SSA concentrations at Arctic sites compared to ground observations even when lead emissions are not included, suggesting underestimation of SSA sinks and/or uncertainties in SSA emissions from blowing snow and open ocean. Multi-year monthly mean surface bromine atom (Br) concentrations increase 2.8-8.8% due to SSA from leads for the 2002-2008 cold season. Changes in ozone concentrations are negligible. While leads contribute <10% to Arctic-wide SSA emissions in the years 2002-2008, these emissions occur in regions of low background aerosol concentrations. Leads may increase in frequency under future climate change, which could increase SSA emissions from leads.

Short Summary

There is uncertainty in the sources of Arctic cold season (November-April) sea salt aerosols. Using a chemical transport model and satellite observations, we quantify Arctic-wide sea salt aerosol emissions from fractures in sea ice, called open sea ice leads, and their atmospheric

chemistry impacts for the cold season. We show sea ice leads contribute to Arctic sea salt aerosols and bromine, especially in under-observed regions.

1. Introduction

Sea salt aerosols (SSA) affect Arctic climate by scattering incoming solar radiation and acting as cloud condensation nuclei and ice nuclei (DeMott et al., 2016; Pierce and Adams, 2006; Quinn et al., 1998). While in the Arctic there is no sunlight during polar night to scatter radiation, cloud condensation nuclei and ice nuclei can still have impacts on clouds and longwave radiation. Long-term measurements have shown that peak SSA concentrations in the Arctic occur during the cold season (Leaitch et al., 2018; Quinn et al., 2002; Schmale et al., 2021). However, the sources and mechanisms of cold season SSA emissions are uncertain, which hinders atmospheric chemistry and climate models from accurately representing polar regions. Recent observations from Utqiaġvik, Alaska have suggested that open leads, or open sea ice fractures, are an important source of cold season SSA emissions (Kirpes et al., 2019; May et al., 2016). Climate change has impacted the Arctic by rapidly decreasing sea ice age and thickness (Intergovernmental Panel On Climate Change, 2023; Sumata et al., 2023; Vaughan et al., 2013), and future projections indicate this will continue (Intergovernmental Panel On Climate Change, 2023), suggesting the amount of open leads will increase in the future due to thinner ice that is prone to fracture. More work is needed to discern the Arctic-wide importance and impacts of SSA emissions from sea ice leads ("lead emissions") on atmospheric chemistry and climate. By combining satellite observations and chemical transport modeling, we quantify the significance and impacts of lead emissions on atmospheric concentrations of SSA and bromine and evaluate simulated SSA against in-situ observations.

While global models have not yet included SSA emissions from leads, several observational studies largely based in Utqiaġvik, Alaska suggest emissions of SSA from leads may be important. Key early observations in the 1970s in Utqiaġvik by Scott & Levin (1972) and Radke et al. (1976) demonstrated an increase in sodium-containing particles in the presence of open water leads. Since then, more recent measurement studies have quantified SSA emissions from leads. Nilsson et al. (2001) estimate that leads contribute an order of magnitude less than the open ocean to the Arctic SSA flux during the summer months. A multi-year study of observed SSA at Utqiaġvik (May et al., 2016), conducted over all seasons, found that leads are a significant contributor to SSA through wind-driven production, increasing the supermicron range in particular,

but to a lesser extent than wind-driven production from the open ocean. Willis et al. (2018) suggest that lead emissions are more important in winter and early spring as winds over the Northern oceans are at their highest. Kirpes et al. (2019) also convey the importance of seasonality, identifying SSA produced by local leads as the dominant aerosol source in the coastal Alaskan Arctic during winter months. Chen et al. (2022), focusing on the spring at Utqiaġvik, shows leads were present locally throughout the study and contributed to sea spray aerosol production. As ground-based observations in the Arctic are mainly limited to coastal stations, such as Utqiaġvik, it is difficult to estimate the significance and impacts of lead emissions over the entire Arctic. Representing Arctic-wide emissions from leads in a global chemical transport model, especially during the cold season, will help discern whether lead emissions and their impacts on atmospheric chemistry are significant enough to warrant inclusion in chemistry as well as climate models.

Other modeling studies in the Arctic and observations primarily from Antarctica suggest blowing snow is a potential major contributor of cold season SSA in polar regions. Blowing snow SSA comes from saline snow over sea ice that is swept up by wind; the snow becomes salty through the upward movement of brine from sea ice to the snow surface, incorporation of frost flowers, and deposition of SSA from the nearby open ocean (Domine et al., 2004). In two chemical transport models, the inclusion of additional SSA emissions from blowing snow brought simulated SSA mass concentrations closer to what was observed (Confer et al., 2023; Huang et al., 2018; Huang and Jaeglé, 2017; Rhodes et al., 2017). Other potential sources of cold season SSA, such as frost flowers, have been found to be insignificant (Alvarez-Aviles et al., 2008; Roscoe et al., 2011; Yang et al., 2017). Incorporating blowing snow SSA emissions into models has shown how missing sources of SSA in the Arctic can have a significant impact on atmospheric chemistry; for example, Huang et al. (2020) show bromine released by blowing snow impacts modeled springtime bromine activation and ozone depletion events. The strong observational evidence that leads contribute to cold season SSA and the impact of blowing snow SSA on modeled Arctic atmospheric chemistry suggests there is a need to assess the potential impacts of lead emissions, which are currently missing from global chemistry and climate models. One study incorporated SSA emissions from leads in a chemical transport model (WRF-Chem), but the study was limited to the 400 km^2 area surrounding Utqiaġvik, Alaska and used ERA-5 reanalysis sea ice fraction to define the presence of leads (Ioannidis et al., 2023). They find open leads are the primary source of fresh and aged SSA in Utqiaġvik, Alaska during the cold season, consistent with the observational analyses by May et al. (2016) and Kirpes et al. (2019).

SSA play a critical role in Arctic tropospheric chemistry. SSA debromination is the main global source of reactive bromine in the troposphere (Wang et al., 2021). Reactive bromine chemistry has been attributed to the rapid depletion of ozone in the Arctic springtime, which reaches a maximum in March-April (Simpson et al., 2007). In particular, bromine atom (Br) is key to these ozone depletion events; it is produced through the photolysis of Br_2, which is sourced from SSA debromination and snowpack chemistry (Abbatt et al., 2012; Dibb et al., 2010; Pratt et al., 2013; Stutz et al., 2011). Swanson et al. (2022) show improved springtime model-observation agreement of BrO by including a snowpack photochemistry mechanism based on multiple field observations in a global chemical transport model. While on a global scale, reaction of OH with other SSA-sourced bromine species can also produce Br (Wang et al., 2021), this is minor in polar regions due to low OH concentrations. Br rapidly depletes ozone through heterogeneous reactions, which produces BrO that can photolyze to reform Br, creating a catalytic ozone-depletion cycle (Simpson et al., 2007).

Here, we estimate the pan-Arctic contribution of leads to total SSA emissions during the cold season for the years 2002-2008, by using satellite observations of lead area to parameterize lead-based SSA production in the global chemical transport model GEOS-Chem. We evaluate simulated SSA concentrations against observations and predict the impacts of lead SSA emissions on atmospheric chemistry, including concentrations of Br and ozone.

2. Methods

2.1 Satellite Data of Lead Area Fractions

In this study, we use satellite data of lead area fractions to inform the GEOS-Chem chemical transport model (next section) of where leads are present. The Advanced Microwave Scanning Radiometer-Earth Observation System (AMSR-E) sensor aboard NASA's Aqua satellite recorded brightness temperatures from Earth from 2002-2011 at six different frequencies (https://www.cen.uni-hamburg.de/en/icdc/data/cryosphere/lead-area-fraction-amsre.html) (Integrated Climate Data Center (ICDC) et al., n.d.), which are converted to lead area fractions following the algorithm of Röhrs and Kaleschke (2012). This method of detection can only be applied to the Arctic freezing season (November-April) due to surface melt of the sea ice modifying the sea ice emissivity from May-October, which affects the lead detection algorithm. Daily data is available at 6.25 km horizontal resolution, as the algorithm is not limited by cloud cover. The

AMSR-E satellite data is regridded to 0.5°x0.625° from 6.25x6.25 km using a distance-weighted average remapping for consistency with the emission model's resolution (see Sect. 2.2 below for model details). For the rare individual days with missing data in the dataset (0.8%), we use the average lead area fraction for that month. The lead area fraction includes open water leads and thin ice-covered leads 3 km and wider. The data spans latitudes 41° to 90°N, though a majority of Arctic sea ice lies above 60°N and leads are therefore unlikely to be present at lower latitudes.

We use the AMSR-E lead area product for this study as it avoids cloud interference when detecting leads and provides nearly consistent daily resolution. A limited quantitative validation by Röhrs and Kaleschke (2012) of one day (March 21, 2006) of the AMSR-E product against Moderate Resolution Image Spectroradiometer (MODIS) showed 50% of the total lead area visible in 500 m MODIS images was detected in the AMSR-E product. Leads greater than 3 km in size ("large leads") were detected with certainty for the AMSR-E product (Röhrs and Kaleschke, 2012), so our results effectively estimate emissions from large leads only.

2.2 GEOS-Chem: global chemical transport model

Here we use the 3-D atmospheric transport model GEOS-Chem (geos-chem.org) version 13.2.1 (https://doi.org/10.5281/zenodo.5500717). Within GEOS-Chem, the Harmonized Emissions Component (HEMCO) computes emissions for different sources, regions, and species (Keller et al., 2014). GEOS-Chem and HEMCO are driven by Modern-Era Retrospective Analysis for Research and Applications (MERRA-2) (Gelaro et al., 2017) meteorological fields from the NASA Global Modeling and Assimilation Office (GMAO), which is reanalysis meteorological data assimilated from various observational sources (i.e., satellite, aircraft campaigns, and ground stations) providing variables such as temperature, wind, precipitation, and humidity. GEOS-Chem represents one-way interactions between the MERRA-2 meteorology and chemical constituents, meaning the meteorological conditions can affect the concentration of chemical species but not vice versa.

SSA emissions calculations for the open ocean use a wind- (Gong, 2003; Monahan et al., 1986)- and sea-surface-temperature-dependent (Jaeglé et al., 2011) source function. In polar regions, SSA emissions from blowing snow are also included (Huang and Jaeglé, 2017). SSA have two size bins: coarse mode (SALC; r= 0.5 to 10 μm) and accumulation mode (SALA; r= 0.1 to 0.5 μm). For gas and aerosol species, wet deposition (both rain and snow) includes washout and

rainout in convective and large-scale stratiform precipitation (Amos et al., 2012; Liu et al., 2001; Wang et al., 2014). From November to April in the Arctic, wet deposition is mainly in the form of snow (Screen and Simmonds, 2012). Dry deposition of gas and aerosol species follows a resistance-in-series approach, and includes gravitational settling of sea salt (Jaeglé et al., 2011; Pound et al., 2020; Wang et al., 1998; Zhang et al., 2001). Coupled gas- and multiphase-reactive halogen chemistry, including sea salt debromination, acid displacement, and photolysis and oxidation of gas-phase inorganic bromine and chlorine species, is described in Wang et al. (2021). This version of GEOS-Chem does not include snowpack chemistry as a source of reactive bromine in the standard model.

We parameterize SSA emissions from leads with the same function as the open ocean emissions from Jaeglé et al. (2011) (Eq. (S1) in the Supplemental Information (SI)), scaled by the fractional area of leads in each grid cell from the AMSR-E satellite data. The Jaeglé et al. (2011) function is empirically derived to best match global observations in GEOS-Chem. We assume that leads emit SSA at an equal rate as a function of lead area. This lead emissions parameterization is a unique wind- and SST-dependent source function for calculating lead emissions, driven by satellite observations defining the presence of leads. Figure 1 shows an example of the daily temporal frequency and spatial resolution of the AMSR-E satellite data (both the raw (a) and regridded (b)) used to drive the model.

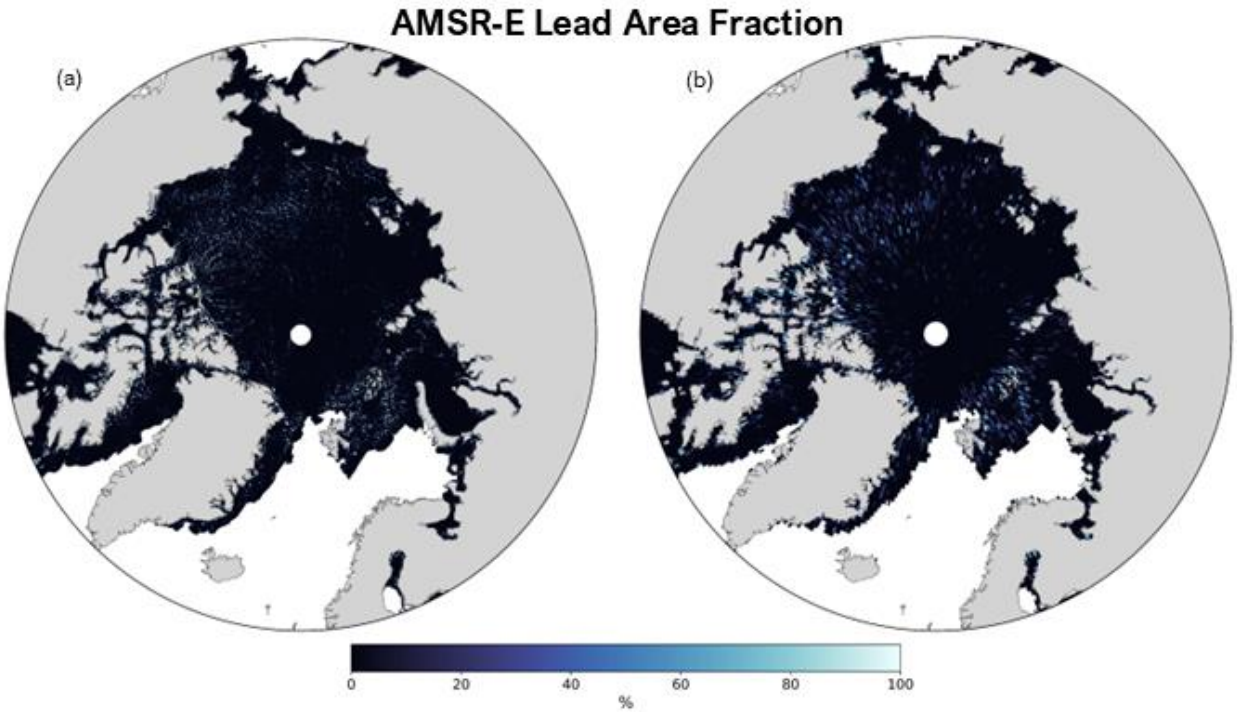

Figure 1- Map of AMSR-E daily lead area fraction in percent (%) for November 1, 2002, both raw (6.25-km resolution) (a) and re-gridded (0.5˚x0.625˚ resolution) (b).

We first calculate SSA emissions at the highest resolution of HEMCO (0.5°x0.625°), which is the native resolution of MERRA-2. Two sets of emissions are calculated: (1) the standard emissions only (i.e., open ocean and blowing snow SSA emissions, the "standard" case); (2) SSA emissions with lead emissions added ("standard + leads" case). Each set of emissions are then implemented separately into GEOS-Chem "offline" to ensure total SSA emissions are properly scaled and distributed and not influenced by the resolution-dependence of the wind speed (Lin et al., 2021). GEOS-Chem is run at the highest global horizontal (2° latitude x 2.5° longitude) and vertical (72 vertical levels) resolution. The absolute difference between the standard + leads and standard simulations is the change in SSA emissions or concentration from leads, and we present the percent change due to leads (%) as calculated with Eq. (1).

$$Percent\ change\ due\ to\ leads\ (\%) = 100 \times \frac{(Standard+leads)_{simulation} - (Standard)_{simulation}}{(Standard)_{simulation}} \quad (1)$$

Simulations are performed for the years 2002-2008, when there is overlap between the AMSR-E satellite data and available observed Arctic SSA concentrations at multiple sites, following one year of initialization. Because satellite observations of lead area fractions begin November 1,

2002, we initialize the standard + leads case for GEOS-Chem with standard + leads SSA emissions for one year (November 1, 2002 to November 1, 2003) and then start the simulation for analysis on November 1, 2002, with the spun-up November 1, 2003, initial conditions. For the standard case, the initialization year begins November 1, 2001. For both cases, we simulate SSA concentrations, evaluate against observed concentrations, and assess the impacts of additional lead emissions on atmospheric chemistry. This includes analysis of the change in atmospheric concentrations of bromine atom (Br) and ozone (O_3). For model evaluation, GEOS-Chem does not track sodium (Na^+) content for SSA, so we convert simulated SSA to Na^+ mass concentrations using a factor of $\frac{1}{3.256}$, which is based on the mass ratio of Na^+ in seawater (Confer et al., 2023; Huang and Jaeglé, 2017; Riley and Chester, 1971).

2.3 In-Situ Observations of Arctic Sea Salt Aerosol Concentrations

We evaluate simulated concentrations of SSA from GEOS-Chem, converted to Na^+ concentrations, against in situ observations of Na^+ concentrations at 4 Arctic sampling sites: Utqiaġvik, Alaska (71.3°N, 156.6°W; 11m a.s.l.) (Quinn et al., 2002); Zeppelin Mountain, Svalbard, Norway (78.9°N, 11.9°E; 475m a.s.l.) (World Meteorological Organization (WMO), 2003); Alert, Nunavut, Canada (82.5°N, 62.5°W; 210m a.s.l.) (World Meteorological Organization (WMO), 2003); Pallas (Matorova), Helsinki, Finland (68 °N, 24.24 °E; 340m a.s.l.) (Salmi, 2018). These observations are available for the time period of this study (November-April from 2002-2008, except for Pallas station, 2003-2008). In winter months, the Utqiaġvik, Zeppelin, and Alert coastal sites border mostly ice-covered ocean (Huang and Jaeglé, 2017). At Utqiaġvik, mass concentrations of Na^+ for submicron and supermicron aerosols are separated, while the other two sites measure the total mass concentration without size distinction. The Na^+ mass concentrations are determined from ion chromatography with uncertainties of 5-11%, or an absolute uncertainty of 0.01 μg/m^3 (Quinn et al., 2000; World Meteorological Organization (WMO), 2003). The aerosol sampling frequency is daily at Zeppelin, Utqiaġvik (submicron), and Pallas and weekly at Alert and Utqiaġvik (supermicron).

3. **Results**

3.1 Emissions of Sea Salt Aerosols from Leads

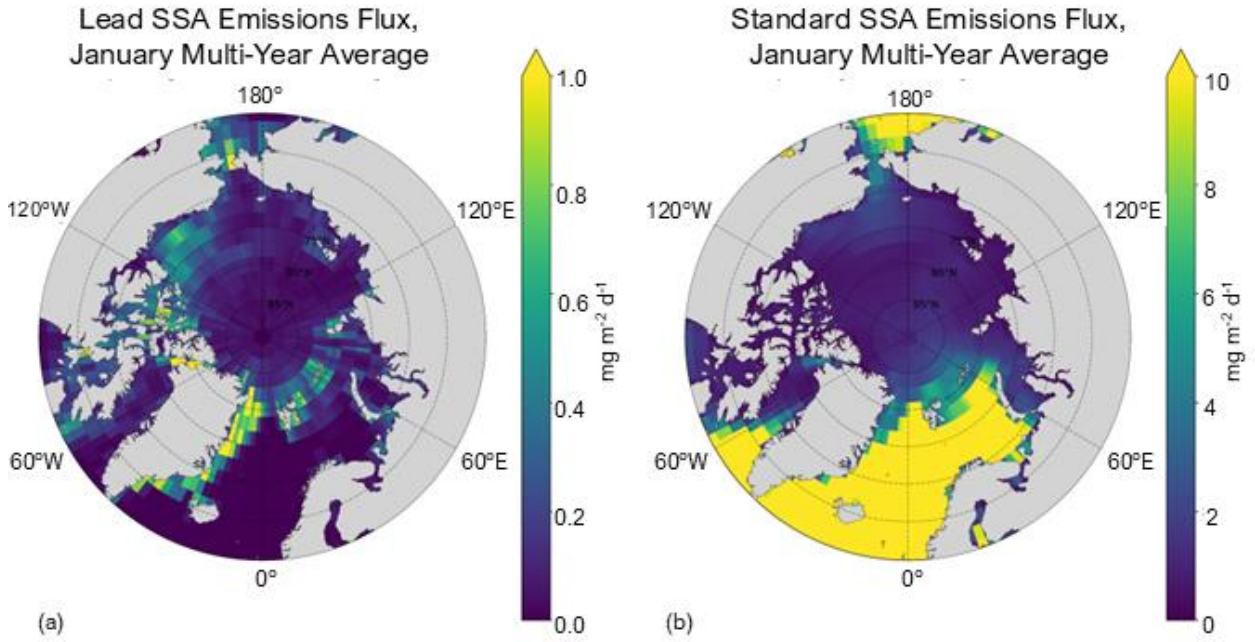

Figure 2- Total (coarse + accumulation mode) lead SSA emissions (a) and standard SSA emissions (b), averaged over 2002-2008 for January. Note the difference in magnitude of the colorbar of (a) and (b).

Figure 2a shows the spatial distribution of multi-year (2002-2008) average lead emissions for the month of January, which is a climatology based on model simulations that use daily resolution lead data (e.g., Fig. 1). We focus Figs. 2 and 4 on the month of January as an example. January is tied for highest lead emissions for latitudes 60°N and greater and second highest for latitudes 75°N and greater (Table 1), and also has the second largest multi-year average lead area (see Fig. S3b in SI). Alongside Fig. 2a is the standard model, which includes open ocean and blowing snow emissions (Fig. 2b; see Sect. 2.2). Total emissions are resolution independent and are shown in Fig. 2 for the 2.0°x2.5° resolution of the online atmospheric chemistry simulation. We find the lead emissions and lead area are spatially consistent (Figs. 1 and 2a) and occur in regions where the standard SSA emissions are low (e.g., in the Greenland Sea and parts of the Barents Sea). The percent change in SSA emissions due to leads (calculated with Eq. (1)) is detailed in Table 1; Figs. 4, 5, and S4 show the percent change in SSA concentration due to leads. Generally, emissions tend to be higher from 70° to 80° N and more concentrated within the Bering Strait, Nares Strait, Wynniatt Bay in the Canadian archipelago, and the eastern Greenland Sea, as opposed to off the coast of Northern Russia and Europe. Month to month, regions where emissions are higher remains similar while the magnitude varies (see Fig. S1 in SI).

Month	Multi-Year (2002-2008) Average Standard Emissions [Gg]		Multi-Year (2002-2008) Average Lead Emissions [Gg] (and corresponding Monthly Percent Change in SSA Emissions due to Leads)	
	≥60°N	**≥75°N**	**≥60°N**	**≥75°N**
November	7800 ± 1000	610 ± 210	82 ± 0.14 (1.1% ± 0.14%)	42 ± 0.13 (6.9% ± 0.13%)
December	8700 ± 1400	640 ± 140	110 ± 0.20 (1.2% ± 0.20%)	48 ±0.32 (7.5% ± 0.32%)
January	8400 ± 1100	670 ± 290	110 ± 0.10 (1.3% ± 0.10%)	46 ± 0.15 (6.9% ± 0.15%)
February	6700 ± 850	510 ± 90	100 ± 0.11 (1.5% ± 0.11%)	37 ± 0.17 (7.2% ± 0.17%)
March	6000 ± 1000	470 ± 66	98 ± 0.074 (1.6% ± 0.07%)	34 ± 0.26 (7.2% ± 0.26%)
April	4200 ± 330	400 ± 61	74 ± 0.081 (1.8% ± 0.08%)	23 ± 0.17 (5.6% ± 0.17%)

Table 1- Multi-year (2002-2008**)** monthly average standard emissions and lead emissions ±1 standard deviation [Gg] and percent change in SSA emissions due to leads ±1 standard deviation in parentheses (calculated using Eq. (1)), averaged for ≥60°N and ≥75°N.

Table 1 shows the standard and lead emissions in Gg as well as the percent change in multi-year monthly average SSA emissions due to leads for 60° to 90°N latitude (≥60°N) and 75° to 90°N (≥75°N**)**. The standard deviations in Table 1 represent the year-to-year variability in emissions, as the calculation is performed across the 7-year simulation time period for each month. Leads are relatively more important to total SSA emissions at higher latitudes due to large open ocean emissions in the North Atlantic at lower latitudes (Table 1; Fig. 2b) and the spatial variability of the lead emissions (Fig. 2a). The month with the highest contribution to SSA emissions from leads varies with the region being analyzed. The smaller magnitude of standard emissions later in the cold season poleward of 60˚ N make lead emissions relatively more important, with the largest

percent increase ≥60˚ N in SSA emissions due to leads occurring in April. Poleward of 75˚ N, the lead emissions represent a larger fraction of the standard emissions, resulting in higher percent increases due to leads (~4-6% higher than for ≥60˚ N). Absolute lead emissions peak in December for ≥75˚ N latitude, which is also the month with the highest percent increase due to leads ≥75˚ N, and decrease more than twofold by April. Controlling factors of the lead emissions are discussed in the next paragraph.

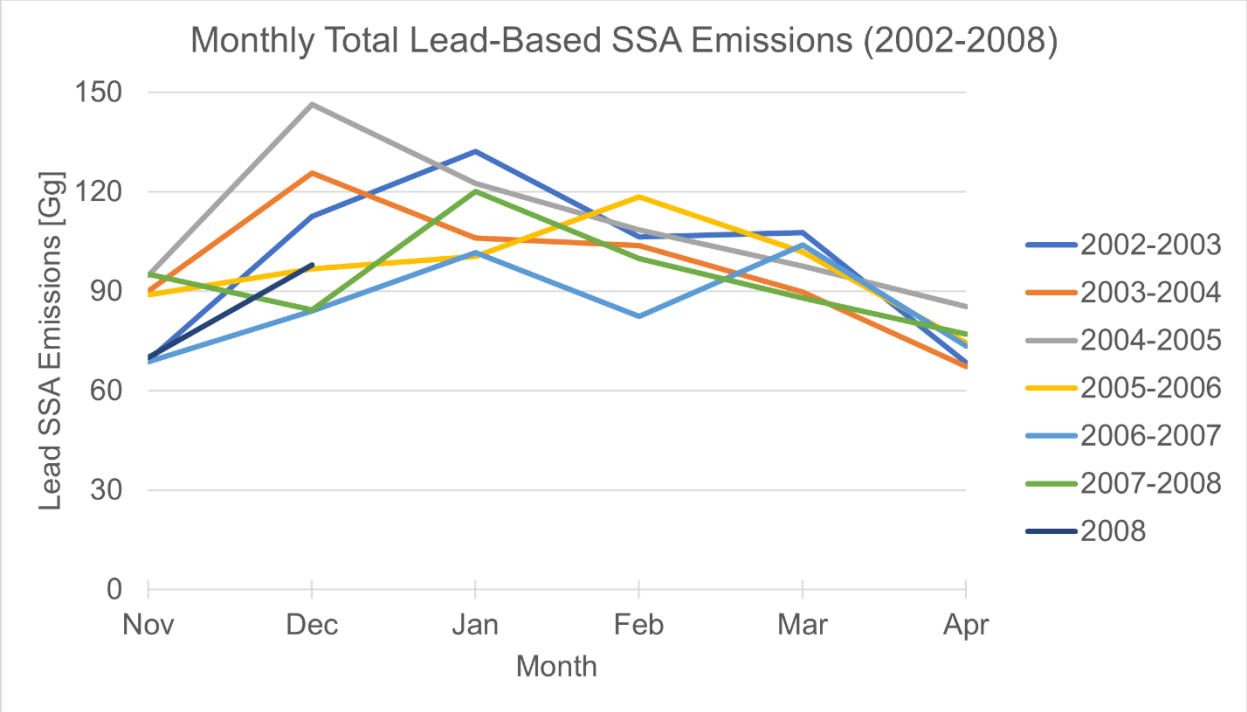

Figure 3- Monthly variations of total (coarse + accumulation mode) lead emissions of SSA during the cold season for 2002-2008. Each line includes November and December of the first year and January through April of the following year, except for the year 2008, which only includes November and December of 2008.

We find that the magnitude of lead emissions varies by month and year, as well as seasonally (see Fig. 3 and Figs. S1 and S2). Monthly total lead emissions and lead area have low correlation (R^2= 0.13, see Fig. S3), indicating the variance in monthly total lead emissions is dominated by the nonlinear dependencies on wind speed and sea surface temperature (Eq. S1 in SI), as the lead emissions are calculated with the Jaegle et al. (2011) wind speed and sea surface temperature source function. In most years, lead emissions decrease from January-April, but there is no single month when lead emissions peak each year (Fig. 3). There is also no clear interannual trend in cold season total lead emissions (see Fig. S2). Lead emissions are lowest in

the 2006-2007 cold season and highest in the 2004-2005 cold season (Fig. S2). In the future, climate models predict that Arctic sea ice will continue to thin (high confidence) and the presence of first-year vs. multi-year sea ice will increase (very high confidence) (Intergovernmental Panel On Climate Change, 2023), suggesting a possible future increasing trend in lead area and therefore lead emissions.

3.2 Atmospheric Chemistry Impacts of Sea Ice Leads

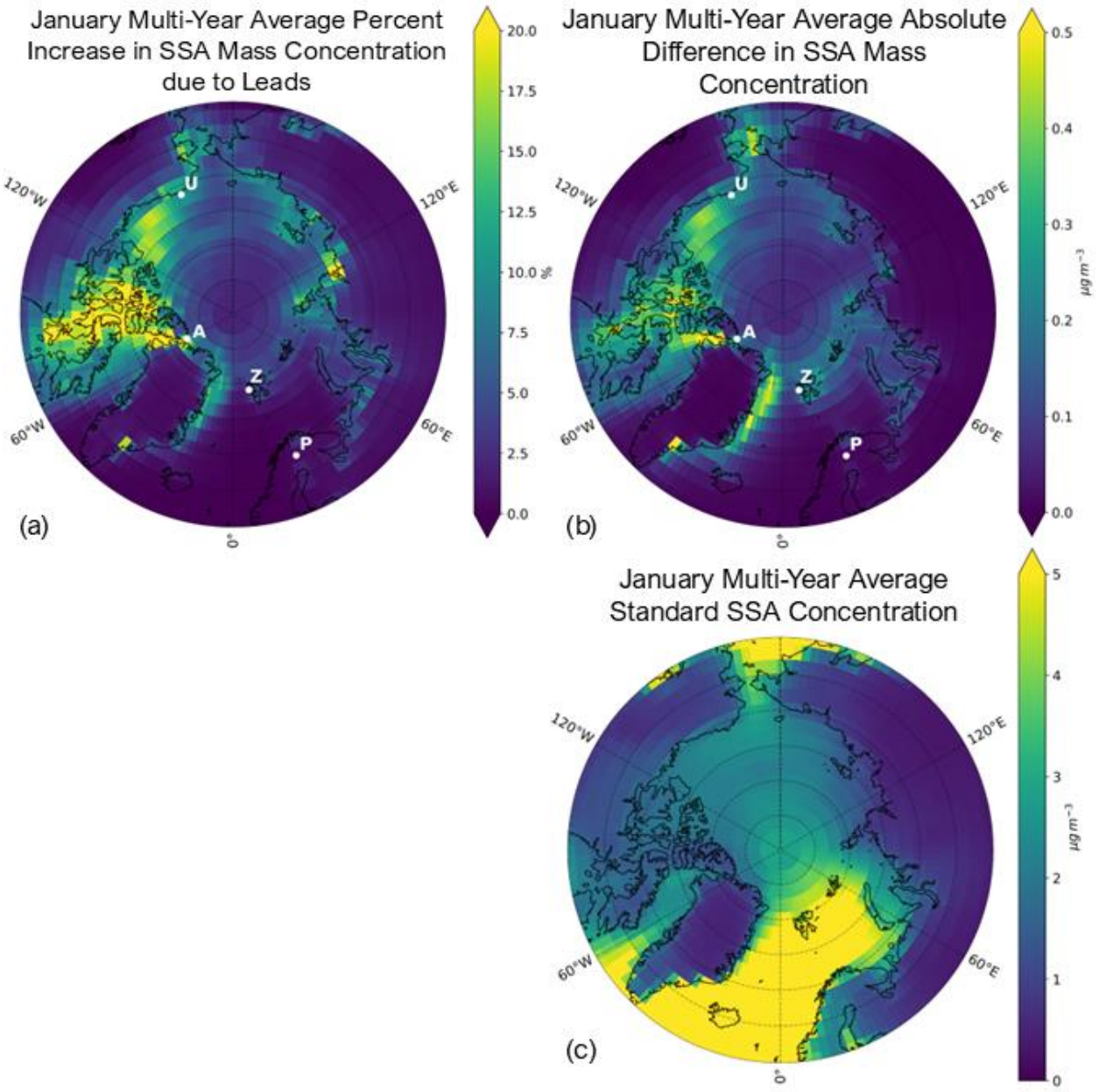

Figure 4- Percent change due to leads (calculated with Eq. (1)) in SSA mass concentration (a), absolute difference between the standard+leads and standard SSA mass concentrations in μg m^{-3} (b), and the standard surface SSA mass concentration in μg m^{-3} (c) for the January multi-year (2002-2008) average. White points in (a) and (b) represent the respective locations of each observational site: Alert, Nunavut, Canada (A); Utqiaġvik, Alaska (U); Zeppelin Mountain, Svalbard, Norway (Z); Pallas (Matorova), Helsinki, Finland (P). Note the difference in magnitude of colorbars (b) and (c).

Figure 4 shows the spatial distribution of the multi-year (2002-2008) average percent change due to leads in surface SSA mass concentration (4a) and the absolute difference in SSA mass concentration between the standard + leads and standard simulations (4b), as well as the standard simulated SSA mass concentration (4c) for the month of January. With the addition of leads, the average Arctic-wide (≥60°N) percent increase in multi-year mean January SSA mass concentrations is 3.3%, and the maximum percent increase in an individual model gridbox is 60.5%. We find that the greatest percent increases due to leads in SSA mass concentrations occur at the location of lead emissions (see Fig. 2a), where the standard concentrations are also very low, except off the eastern coast of Greenland, where the percent increase is reduced due to the high background SSA concentrations in the Greenland Sea (Fig. 4c) from open ocean emissions (Fig. 2b).

Figure 5a shows the average Arctic-wide percent increase and 5c shows the absolute difference due to leads in multi-year monthly mean SSA mass concentration for each cold season month. Averaged poleward of 60°N, the percent increase and absolute difference due to leads in SSA mass concentration remains relatively constant throughout the cold season (Fig. 5a and c). Changes in monthly mean SSA mass concentrations are also higher poleward of 75°N. However, the percent increase in SSA mass concentration for both latitudinal ranges have large spatial variability, as seen in the standard deviation in Fig. 5a. The spatial distribution of the percent increase and absolute difference in SSA mass concentration due to leads remains similar month to month (see Fig. S4 and S5 in SI).

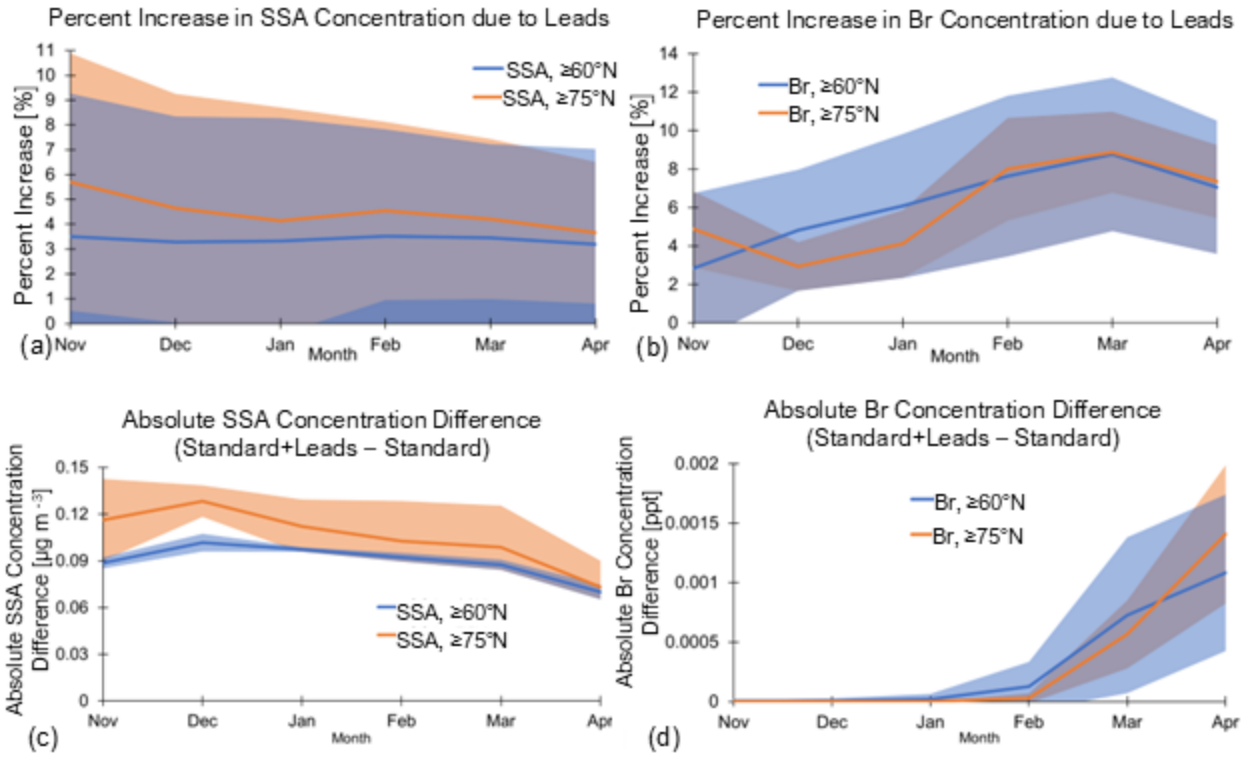

Figure 5. Multi-year (2002-2008) monthly mean percent increase due leads (calculated with Eq. (1)) in surface (a) SSA and (b) Br concentrations averaged across different Arctic regions (blue line: ≥60˚ N; orange line: ≥75˚ N). Shaded area represents ±1 standard deviation.

As described in Sect. 1, SSA contribute to the production of tropospheric reactive bromine and thereby bromine atom (Br). Here we examine changes in Br due to its role in ozone depletion events.

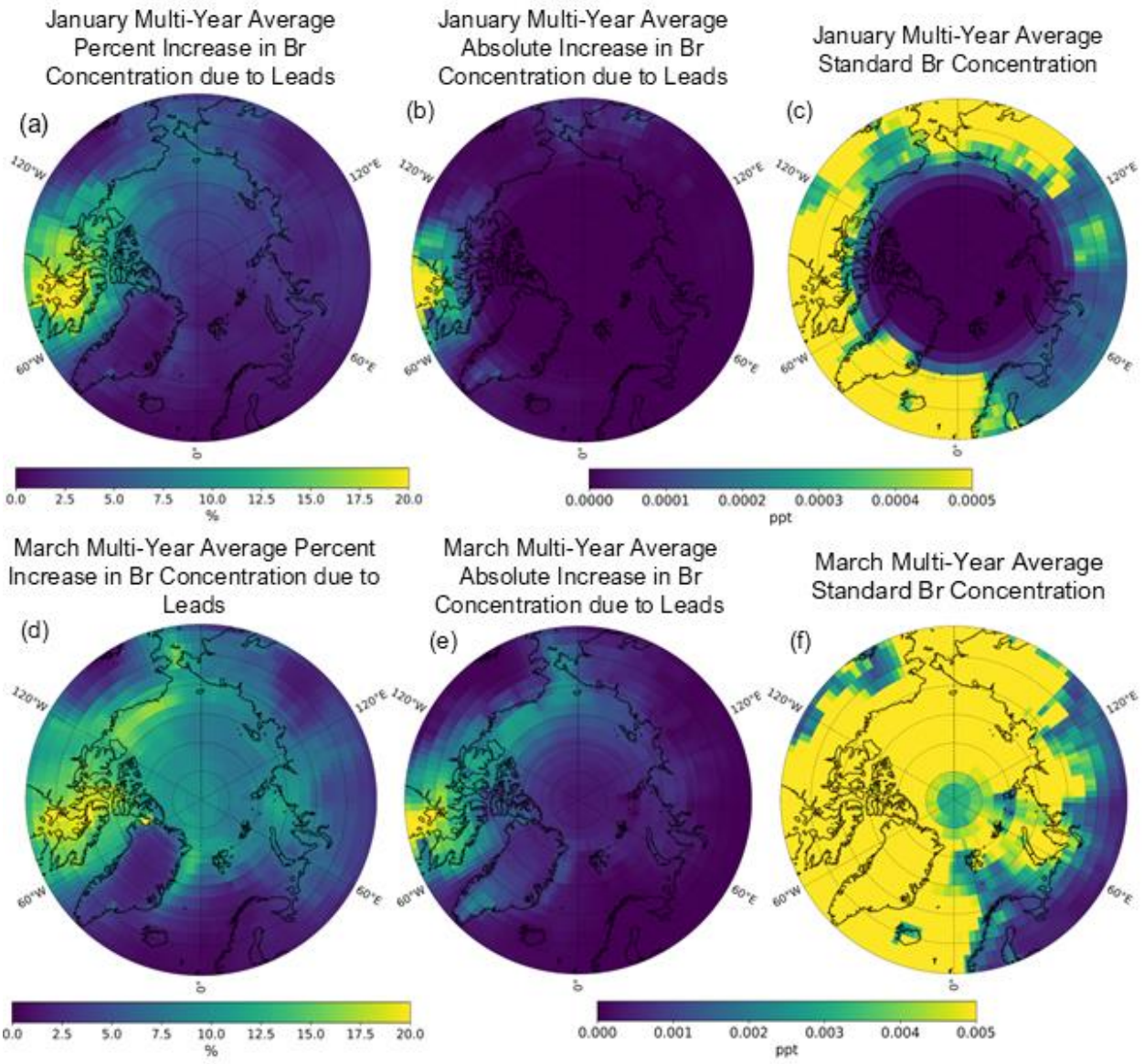

Figure 6- Multi-year (2002-2008) mean January (a, b, and c) and March (d, e, and f) percent increase due to leads in surface Br concentration (a and d), absolute increase in surface Br concentration due to leads (b and e), and the standard model surface Br concentration in ppt (c and f). Note the scale of the absolute difference and standard Br concentrations for the January and March multi-year averages are an order of magnitude difference.

Figure 6 shows the multi-year (2002-2008) mean percent increase and absolute difference due to leads in surface Br concentrations, and the standard Br concentration (in parts per trillion, or ppt) for the months of January (a-c) and March (d-f), respectively. Increased SSA from leads increases surface levels of Br across all months during the cold season (Fig. 6a, b, d, and e; Figs. S6 and S7 in the SI for other months). These increased concentrations spatially follow the

increased SSA mass concentrations from leads (Fig. 4a; Figs. S4 and S5 in SI for other months) with differences due to where Br can be produced photochemically from the precursors released from SSA. The spatial distribution of the percent increases in Br due to leads remains relatively similar month to month during the cold season (see Fig. S6 in SI), but with varying magnitude (Fig. 6). The changes in Br concentration in February to April occur over a larger area (Fig. 6d and e and Figs. S6 and S7), likely due to the seasonality of Arctic bromine chemistry, which is influenced by increasing area where sunlight is available to photolyze Br-sourced SSA species. The average Arctic-wide (≥60°N) percent increase due to leads in multi-year January mean surface Br concentration is 6.1% and the maximum increase in an individual gridbox is 35%; for March, it is 8.8% and 20.4%, respectively. Overall, the average monthly percent increase in Br concentration is higher than the corresponding increases in SSA concentration, particularly after January, and reaches a maximum in March (see Fig. 5). The percent change due to leads in Br concentrations increases from November-March poleward of 60°N and from December-March poleward of 75°N (Fig. 5b). This does not strictly follow the seasonality of lead emissions (Fig. 3) or the percent increase in SSA concentrations due to leads (Fig. 5a), likely due to more available sunlight for photochemical reactions that produce Br later in the cold season. Increases in surface Br concentration could lead to decreased surface ozone concentrations. We find that the percent decrease due to leads in average surface ozone concentrations during the Arctic cold season, however, are negligible (< -0.25%).

3.3 Evaluation Against Sea Salt Aerosol Observations

We compare modeled and observed sodium (Na^+) mass concentrations at four long-term monitoring stations to evaluate the performance of the simulation with and without additional lead emissions. The locations of each observational site are shown in Fig. 4a.

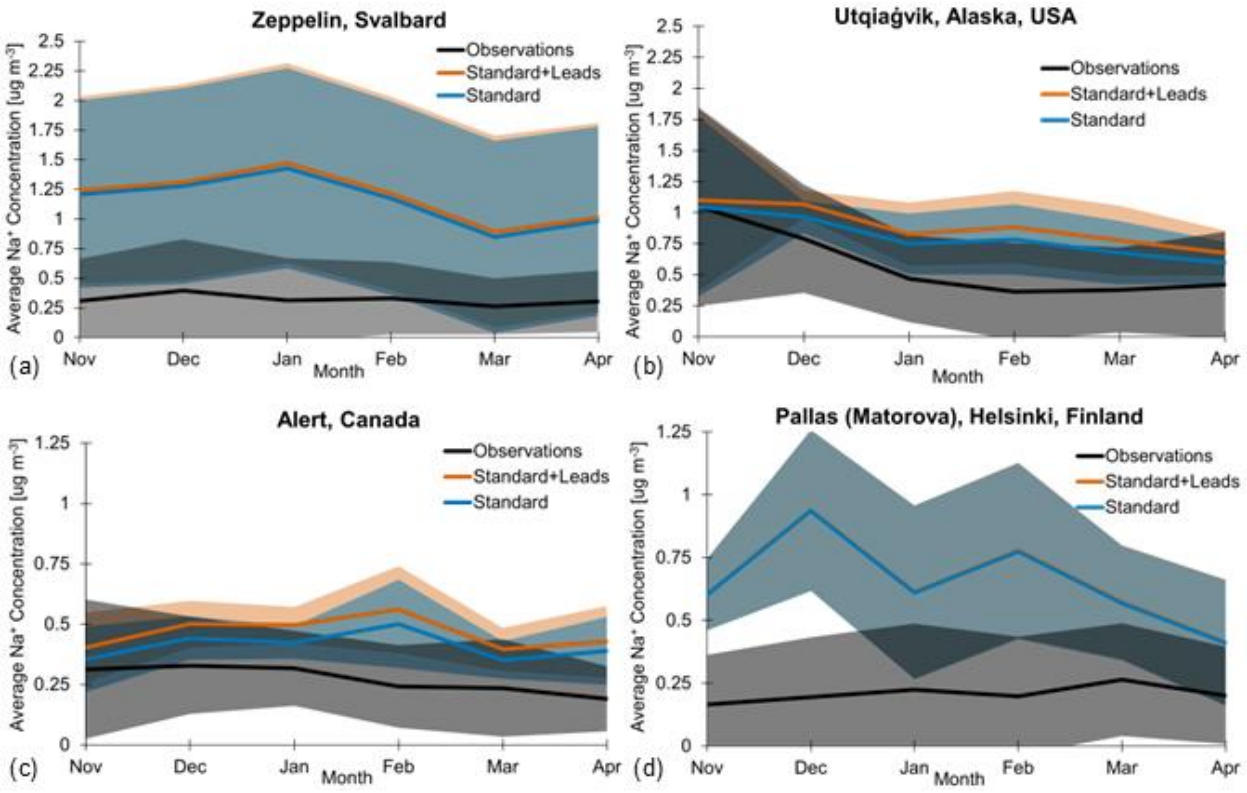

Figure 7- Observed (blackline) and simulated (blue and orange lines) multi-year monthly mean sodium mass concentrations at (a) Zeppelin, Norway, (b) Utqiaġvik, Alaska, (c) Alert, Canada, and (d) Pallas (Matorova), Helsinki, Finland for the cold seasons of 2002-2008 for (a)-(c) and 2003-2008 for (d). Shaded regions are ±1 standard deviation. Note the y-axis for Alert (c) and Pallas (d) are half as large as Zeppelin (a) and Utqiaġvik (b).

Figure 7 shows multi-year monthly mean Na^+ concentrations in the observations (black), standard + leads simulation (orange), and standard simulation (blue) for Zeppelin (a), Utqiaġvik (b), Alert (c), and Pallas (d) during the cold season for 2002-2008 (a-c) and 2003-2008 (d). We sample the model simulations in the gridbox that encompasses the latitude, longitude, and altitude of each monitoring station (see Sect. 2.3) and convert the simulated SSA to Na^+ concentrations. For all sites and months during the cold season, the simulated and observed Na^+ mass concentrations overlap within ± 1 standard deviation (shaded regions in Fig. 7), except in November and December at Pallas. We find mean concentrations are overpredicted in both the standard and standard + leads simulations at all sites and months during the cold season, apart from the standard model at Utqiaġvik and Alert in November which agree closest with observations.

The model overpredicts Na^+ concentrations the most at Zeppelin and Pallas, with the standard + leads and standard mean concentrations a factor of 3.2 to 4.71 and 2.0 to 4.8 higher, respectively, than observations across all months during the cold season. Confer et al. (2023) similarly find an overprediction of SSA at Zeppelin, which they find is exacerbated by including blowing snow emissions. Additionally, Zeppelin is at high elevation (located on a mountain at 475m) and has been found to be more impacted by the free troposphere and aerosol-cloud interactions than other Arctic sites (Freud et al., 2017); the chemical transport model cannot represent two-way aerosol-cloud interactions. The model overestimate is less at Utqiaġvik, where the standard + leads simulation still overpredicts observed concentrations by a factor of 1.0 to 2.4, and least at Alert, with observed concentrations overestimated by a factor of 1.3 to 2.3 for the standard + leads model. Lead emissions do not change the simulated seasonality of cold season surface SSA concentrations. The timing of cold season maximum and minimum concentrations at Zeppelin, Alert, and Pallas differs between the observed and simulated, for both the standard + leads and standard models. At Utqiaġvik, the maximum mass concentration in the observations and both model simulations occurs in November. However, the minimum observed cold season mass concentration occurs in February at Utqiaġvik, whereas the standard + leads and standard mean concentrations reach a minimum in April.

Figure 4a and b places the differences seen at each of the three sites in Fig. 7 into a broader context, with maps of the relative and absolute increases in SSA mass concentrations for the month of January. There is minimal change in SSA concentrations where Pallas is located, explaining the near equal Na^+ concentrations for the standard + leads and standard simulations which results in the overlapping lines in Fig. 7d, suggesting minimal influence from leads at this site likely due to its inland location. The most significant relative increase in SSA concentration from leads out of the four sites occurs at Alert (Fig. 7a). However, regions with the largest changes in SSA mass concentration due to leads in Fig. 4a and b for the month of January (i.e., parts of Northern Canada southwest of Alert), which are consistent throughout the cold season (Fig. S4 and S5 in SI), are not sampled by long-term ground monitoring sites, which would help constrain lead impacts on SSA. In our simulation, lead emissions have the same size distribution as the open ocean, with most of the mass in the coarse mode (82-90%). Despite this, there are increases in SSA concentration over land (Fig. 4a and b) indicating transport (see also Text S2 and Fig. S8). This is consistent with observed inland transport of SSA across the North Slope of Alaska (Simpson et al., 2005). It is likely that leads emit smaller SSA particles relative to open ocean emissions (Nilsson et al., 2001), which would increase their lifetime, so non-local impacts from

leads may be greater than simulated here. This further highlights the need for observations in other regions to better understand the impacts of lead emissions.

There is strong observational evidence that lead emissions contribute to cold season SSA (see Sect. 1), but the standard model consistently overpredicts observed SSA concentrations prior to inclusion of additional lead emissions. This suggests other sources of SSA may be overpredicted or sinks of SSA may be underpredicted. Ongoing work to improve the treatment of aerosol wet removal processes in GEOS-Chem has not specifically investigated the impacts on sea salt aerosol (Luo et al., 2020; Luo and Yu, 2023). Additionally, a recent observational study (Chen et al., 2022) suggests that the GEOS-Chem blowing snow emissions parameterization may overpredict the frequency of blowing snow events, therefore possibly contributing to the overprediction of Arctic SSA mass concentrations.

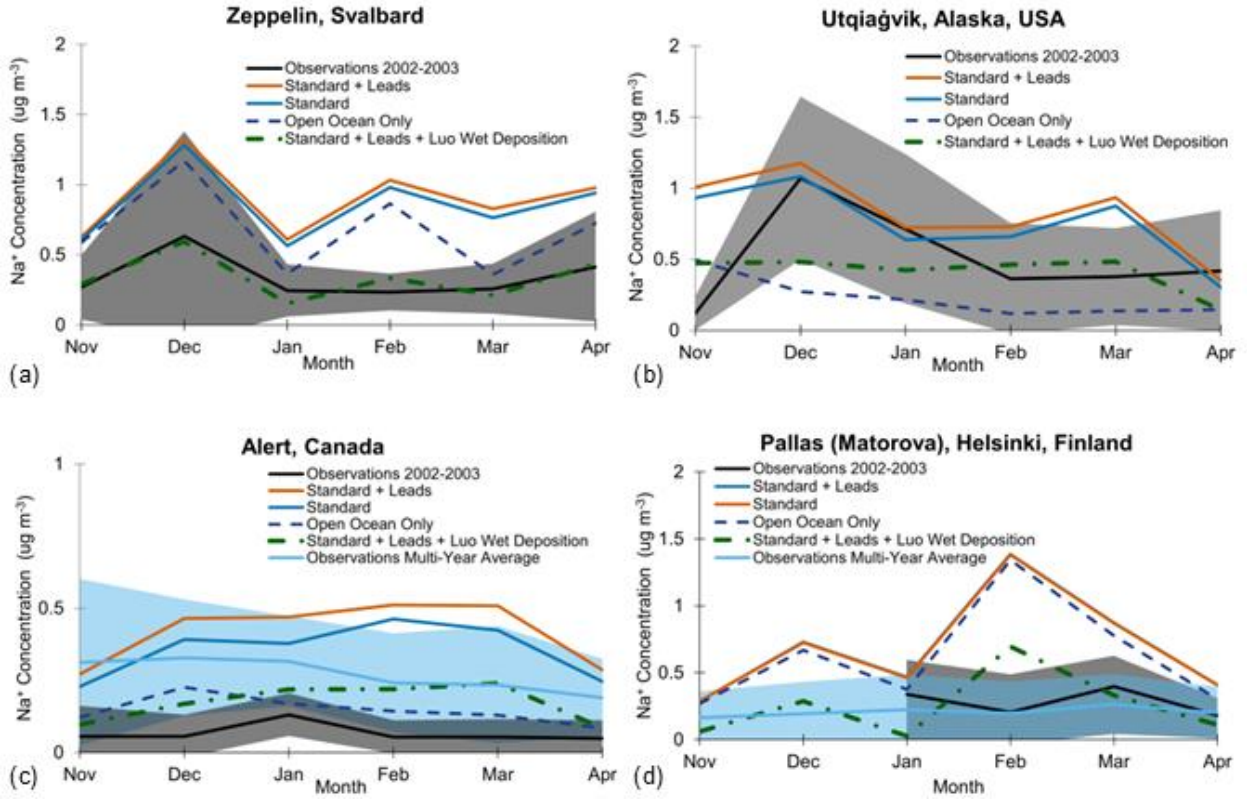

Figure 8- Model evaluation for the cold season 2002-2003 at Zeppelin (a), Utqiaġvik (b), Alert (c), and Pallas (d). Observed Na^+ concentrations are included as monthly averages for 2002-2003 (black + standard deviation margin), and the multi-year monthly averages (light blue + standard deviation margin) (note: no 2002 data is available at Pallas). We show monthly average modeled Na+ concentrations for 2002-2003 for the standard + leads (orange) and standard (blue)

simulations with two additional sensitivity studies: open ocean only emissions contributing to Na+ concentrations (dark blue with dashes) and the standard + leads emissions with Luo et al. (2020) wet deposition applied (green line with dashes + dots). Note the different y-axis for Alert (c), as concentrations are much lower at this site.

To test these possible sources of uncertainty, we run two additional sensitivity simulations for one cold season (November 2002-April 2003): (1) using the Luo et al. (2020) wet deposition scheme with the standard + leads SSA emissions ("standard + leads + Luo Wet Deposition") and (2) turning off blowing snow emissions in the standard model for an "open ocean only" case (see Text S3 for further description). We find that the Luo wet deposition scheme improves model agreement most at Zeppelin (see Fig. 8a), especially in the months of November, December, March, and April. At Utqiaġvik, the Luo wet deposition scheme results in underestimates in Na^+ concentrations compared to observations (Fig. 8b) in December, January, and April and overestimates in November, February, and March; however, the overestimated months are closer to the observed concentrations than the standard + leads and standard simulations. Additionally, the standard model at Utqiaġvik agrees with observations in December and the standard + leads model agrees with observations in January and April.

At Alert, the Luo wet deposition scheme decreases the model overestimate of the standard + leads simulation when compared to the observations for the 2002-2003 cold season (Fig. 8c) but still overestimates Na^+ concentrations in each month. As the 2002-2003 observations at Alert are particularly low, we also include the observed multi-year (2002-2008) monthly average Na^+ concentrations for comparison. The Luo wet deposition scheme improves model evaluation from February-March compared to the multi-year average observed concentrations at Alert, but otherwise underpredicts concentrations. The Luo wet deposition scheme decreases overprediction at Pallas in February compared to observations from the 2003 cold season and improves model agreement in March and April, but underpredicts Na^+ concentrations in January (Fig. 8d). As there are no available observations in 2002 at Pallas, we also include the observed multi-year (2003-2008) monthly average Na^+ concentrations for comparison. The Luo wet deposition scheme underpredicts Na^+ concentrations in November, January, and April and overpredicts concentrations in December and March compared to the multi-year average concentrations at Pallas.

At Utqiaġvik, under predicted Na^+ concentrations with only open ocean emissions (except in November) suggest that this site is influenced by blowing snow emissions and/or lead emissions. Of the four sites, blowing snow is most important and well-represented here, as it also improves the modeled seasonality by correctly representing the December peak in Na^+ concentrations in the standard + leads and standard model; there may be larger uncertainty in the emissions parameterization in other regions. At Zeppelin, Alert, and Pallas, even with open ocean emissions only and the standard wet deposition, the model overestimates Na^+ concentrations for all months during the cold season for 2002-2003, except at Pallas in January, where only open ocean emissions more closely match observations. Moreover, the open ocean only Na^+ concentrations are close in value to the standard + leads and standard concentrations, indicating Pallas is largely influenced by open ocean emissions, rather than blowing snow and lead emissions.

The results of these sensitivity tests suggest that changes to wet scavenging may be more important at higher altitudes, given the improvement in model evaluation at Zeppelin. Yet, the inclusion of the Luo wet deposition scheme to the standard + leads simulation still overestimates concentrations at Alert and generally leads to disagreement with observations at Utqiaġvik and Pallas (except in March and April at Pallas).

4. Uncertainties Discussion

Our model evaluation reveals SSA is overestimated in the standard and standard + leads model at each of the 4 Arctic sampling sites, pointing to possible sources of uncertainty. First, we use the Jaeglé et al. (2011) open ocean function for our lead emissions parameterization as it is the standard SSA emission function in GEOS-Chem that has been previously evaluated across global oceans. However, there are possible differences in the mechanisms and meteorological dependencies of SSA emission from leads vs. the open ocean which could impact the magnitude and spatial patterns of lead emissions. Some potential differences were investigated in a summertime measurement study (Nilsson et al., 2001), where they derive an empirical lead emissions flux equation with an exponential dependence on windspeed and no consideration of SST (Eq. (S2) in SI). They found the emissions rate per area from leads is smaller than that of the open ocean due to lower fetch in leads, which suggests the lead emissions estimated in our study may be an upper limit when considering large leads only (>3km in size); however, this lead fraction detected by AMSR-E may only include 50% of total lead area (Röhrs and Kaleschke, 2012). Additionally, Nilsson et al. (2001) suggest leads emit smaller SSA particles relative to the

open ocean, which would increase their lifetime and transport distance. To create a more robust understanding of the different SSA emission mechanisms from leads vs. the open ocean, more studies using size-resolved observations could be conducted within the areas we predict the highest lead emissions, such as within the Bering Strait, Nares Strait, Wynniatt Bay in the Canadian archipelago, and the eastern Greenland Sea.

Our sensitivity study results do not ultimately confirm the source(s) of overprediction within the GEOS-Chem model. Blowing snow emissions are included as a standard source of SSA emissions in the Arctic, but remaining uncertainties about the GEOS-Chem blowing snow emissions parameterization (Chen et al., 2022) suggest a need for refinement. The results of the standard + leads + Luo wet deposition simulation highlight there are also remaining uncertainties associated with wet deposition schemes as the Luo et al. (2020) mechanism does not lead to consistent improvement of simulated SSA concentrations. Luo & Yu (2023) find that the scheme overestimates wet scavenging on a global scale, so continued improvement in the model deposition processes may resolve SSA overestimates. In addition, there are sparse ground observations of precipitation in the Arctic, and while the MERRA-2 reanalysis uses both model and satellite data to fill these gaps, Arctic cloud properties and precipitation can still be difficult to predict (Barrett et al., 2020; Taylor et al., 2019), which could affect the accurate simulation of aerosol deposition and, in turn, our simulated SSA concentrations.

5. **Conclusions**

Observational evidence (Chen et al., 2022; Kirpes et al., 2019; May et al., 2016; Radke et al., 1976; Scott and Levin, 1972; Willis et al., 2018) and one modeling study of the 400 km^2 region around Utqiaġvik, Alaska (Ioannidis et al., 2023) have shown that leads may be an important source of cold season SSA for the coastal Arctic. Here, we evaluate their importance as an Arctic-wide source of cold season SSA emissions and their potential atmospheric chemistry impacts in the global chemical transport model GEOS-Chem.

We find that lead SSA emissions occur primarily in regions where other SSA emissions sources are very low, mainly within the Bering Strait, Nares Strait, Wynniatt Bay in the Canadian archipelago, and the eastern Greenland Sea. Poleward of 75˚ N, leads increase total monthly cold-season SSA emissions by 5.6 to 7.5%, with the highest contribution of SSA emissions from leads in January and the lowest in April. Lead emissions vary in magnitude by month and year,

mainly due to variations in lead area. Future trends in Arctic sea ice predicted by climate models suggest a possible future increasing trend in lead area (Intergovernmental Panel On Climate Change, 2023), which would increase lead emissions. The additional SSA from leads in regions where the background aerosol concentrations are low could also affect local aerosol-cloud interactions, but the overall warming or cooling effect of these additional aerosols remains uncertain (Cox et al., 2015; Schmale et al., 2021; Stramler et al., 2011; Tan et al., 2023; Villanueva et al., 2022).

SSA mass concentrations increase primarily at the location of lead emissions, in regions where the standard SSA mass concentration is very low (≤1.2 μg m^{-3}). Throughout the cold season, the increased SSA mass concentrations from leads remain relatively constant in magnitude and spatial distribution. The highest increase in multi-year average SSA mass concentrations due to leads, spatially averaged for ≥75°N, occurs in November (5.7% ± 5.2%) and the lowest occurs in April (3.7% ± 2.9%). Increased SSA from leads increases surface Br concentrations during the cold season in corresponding locations. We find total Arctic-wide (≥60°N) increases in multi-year mean surface Br concentration range from 2.8 to 8.8%. The increases in Br are not sufficient to have an impact on ozone; subsequent decreases in average surface ozone concentrations in the Arctic are negligible (< -0.25%).

Overall, we predict sea ice leads may impact Arctic-wide cold-season SSA concentrations and Br concentrations by up to 5-10% on average during the 2002-2008 period. As leads are likely to increase in prevalence under climate change, including this source of SSA in chemistry and climate models may become more important for future predictions.

Code and Data Availability

Standard model code: https://doi.org/10.5281/zenodo.5500717; AMSR-E data: https://www.cen.uni-hamburg.de/en/icdc/data/cryosphere/lead-area-fraction-amsre.html); observational site data (Alert, Pallas, and Zeppelin): https://ebas-data.nilu.no/Default.aspx; observational data (Utqiaġvik): https://saga.pmel.noaa.gov/data/stations/; model data shown in paper: https://doi.org/10.5281/zenodo.14611355.

Author Contribution

EJE was responsible for data curation, model simulations, validation, visualization, and analysis with expert advice from HMH. HMH is responsible for conceptualization. EJE drafted the manuscript which was revised by HMH.

Competing Interests

The authors declare that they have no conflict of interest.

Acknowledgements

We thank Kerri Pratt for helpful discussions. HMH was supported by Department of Energy (DOE) Atmospheric Systems Research (ASR), award DE-SC0023049. We acknowledge financial support from the department of Civil and Environmental Engineering at the University of Illinois Urbana-Champaign.

Supplemental Information

Equations of SSA flux from Jaegle et a. (2011) and Nilsson et al. (2001); Additional figures of lead SSA emissions for months other than January during the cold season; Cold season total lead SSA emissions; Description and figure of the correlation between lead area and lead SSA emissions; long-term trends in lead area (2002-2011) and relevant statistical testing; additional figures of multi-year (2002-2008) mean percent increase due to leads in SSA and bromine concentration for months other than January during the cold season; Description and figures of correlation between lead emissions and coarse and accumulation mode SSA concentration; Sensitivity simulations.

6. References

Abbatt, J. P. D., Thomas, J. L., Abrahamsson, K., Boxe, C., Granfors, A., Jones, A. E., King, M. D., Saiz-Lopez, A., Shepson, P. B., Sodeau, J., Toohey, D. W., Toubin, C., Von Glasow, R., Wren, S. N., and Yang, X.: Halogen activation via interactions with environmental ice and snow in the polar lower troposphere and other regions, Atmospheric Chem. Phys., 12, 6237–6271, https://doi.org/10.5194/acp-12-6237-2012, 2012.

Alvarez-Aviles, L., Simpson, W. R., Douglas, T. A., Sturm, M., Perovich, D., and Domine, F.: Frost flower chemical composition during growth and its implications for aerosol production and bromine activation, J. Geophys. Res. Atmospheres, 113, 2008JD010277, https://doi.org/10.1029/2008JD010277, 2008.

Amos, H. M., Jacob, D. J., Holmes, C. D., Fisher, J. A., Wang, Q., Yantosca, R. M., Corbitt, E. S., Galarneau, E., Rutter, A. P., Gustin, M. S., Steffen, A., Schauer, J. J., Graydon, J. A., Louis, V. L. St., Talbot, R. W., Edgerton, E. S., Zhang, Y., and Sunderland, E. M.: Gas-particle partitioning of atmospheric Hg(II) and its effect on global mercury deposition, Atmospheric Chem. Phys., 12, 591–603, https://doi.org/10.5194/acp-12-591-2012, 2012.

Barrett, A. P., Stroeve, J. C., and Serreze, M. C.: Arctic Ocean Precipitation From Atmospheric Reanalyses and Comparisons With North Pole Drifting Station Records, J. Geophys. Res. Oceans, 125, e2019JC015415, https://doi.org/10.1029/2019JC015415, 2020.

Chen, Q., Mirrielees, J. A., Thanekar, S., Loeb, N. A., Kirpes, R. M., Upchurch, L. M., Barget, A. J., Lata, N. N., Raso, A. R. W., McNamara, S. M., China, S., Quinn, P. K., Ault, A. P., Kennedy, A., Shepson, P. B., Fuentes, J. D., and Pratt, K. A.: Atmospheric particle abundance and sea salt aerosol observations in the springtime Arctic: a focus on blowing snow and leads, Atmospheric Chem. Phys., 22, 15263–15285, https://doi.org/10.5194/acp-22-15263-2022, 2022.

Confer, K. L., Jaeglé, L., Liston, G. E., Sharma, S., Nandan, V., Yackel, J., Ewert, M., and Horowitz, H. M.: Impact of Changing Arctic Sea Ice Extent, Sea Ice Age, and Snow Depth on Sea Salt Aerosol From Blowing Snow and the Open Ocean for 1980–2017, J. Geophys. Res. Atmospheres, 128, e2022JD037667, https://doi.org/10.1029/2022JD037667, 2023.

Cox, C. J., Walden, V. P., Rowe, P. M., and Shupe, M. D.: Humidity trends imply increased sensitivity to clouds in a warming Arctic, Nat. Commun., 6, 10117, https://doi.org/10.1038/ncomms10117, 2015.

DeMott, P. J., Hill, T. C. J., McCluskey, C. S., Prather, K. A., Collins, D. B., Sullivan, R. C., Ruppel, M. J., Mason, R. H., Irish, V. E., Lee, T., Hwang, C. Y., Rhee, T. S., Snider, J. R., McMeeking, G. R., Dhaniyala, S., Lewis, E. R., Wentzell, J. J. B., Abbatt, J., Lee, C., Sultana, C. M., Ault, A. P., Axson, J. L., Diaz Martinez, M., Venero, I., Santos-Figueroa, G., Stokes, M. D., Deane, G. B., Mayol-Bracero, O. L., Grassian, V. H., Bertram, T. H., Bertram, A. K., Moffett, B. F., and Franc, G. D.: Sea spray aerosol as a unique source of ice nucleating particles, Proc. Natl. Acad. Sci., 113, 5797–5803, https://doi.org/10.1073/pnas.1514034112, 2016.

Dibb, J. E., Ziemba, L. D., Luxford, J., and Beckman, P.: Bromide and other ions in the snow, firn air, and atmospheric boundary layer at Summit during GSHOX, Atmospheric Chem. Phys., 10, 9931–9942, https://doi.org/10.5194/acp-10-9931-2010, 2010.

Domine, F., Sparapani, R., Ianniello, A., and Beine, H. J.: The origin of sea salt in snow on Arctic sea ice and in coastal regions, Atmospheric Chem. Phys., 4, 2259–2271, https://doi.org/10.5194/acp-4-2259-2004, 2004.

Freud, E., Krejci, R., Tunved, P., Leaitch, R., Nguyen, Q. T., Massling, A., Skov, H., and Barrie, L.: Pan-Arctic aerosol number size distributions: seasonality and transport patterns, Atmospheric Chem. Phys., 17, 8101–8128, https://doi.org/10.5194/acp-17-8101-2017, 2017.

Gelaro, R., McCarty, W., Suárez, M. J., Todling, R., Molod, A., Takacs, L., Randles, C. A., Darmenov, A., Bosilovich, M. G., Reichle, R., Wargan, K., Coy, L., Cullather, R., Draper, C., Akella, S., Buchard, V., Conaty, A., Da Silva, A. M., Gu, W., Kim, G.-K., Koster, R., Lucchesi, R., Merkova, D., Nielsen, J. E., Partyka, G., Pawson, S., Putman, W., Rienecker, M., Schubert, S. D., Sienkiewicz, M., and Zhao, B.: The Modern-Era Retrospective Analysis for Research and Applications, Version 2 (MERRA-2), J. Clim., 30, 5419–5454, https://doi.org/10.1175/JCLI-D-16-0758.1, 2017.

Gong, S. L.: A parameterization of sea-salt aerosol source function for sub- and super-micron particles, Glob. Biogeochem. Cycles, 17, 2003GB002079, https://doi.org/10.1029/2003GB002079, 2003.

687 Huang, J. and Jaeglé, L.: Wintertime enhancements of sea salt aerosol in polar regions consistent with a
688 sea ice source from blowing snow, Atmospheric Chem. Phys., 17, 3699–3712,
689 https://doi.org/10.5194/acp-17-3699-2017, 2017.

690 Huang, J., Jaeglé, L., and Shah, V.: Using CALIOP to constrain blowing snow emissions of sea salt aerosols
691 over Arctic and Antarctic sea ice, Atmospheric Chem. Phys., 18, 16253–16269,
692 https://doi.org/10.5194/acp-18-16253-2018, 2018.

693 Huang, J., Jaeglé, L., Chen, Q., Alexander, B., Sherwen, T., Evans, M. J., Theys, N., and Choi, S.: Evaluating
694 the impact of blowing-snow sea salt aerosol on springtime BrO and O₃ in the
695 Arctic, Atmospheric Chem. Phys., 20, 7335–7358, https://doi.org/10.5194/acp-20-7335-2020, 2020.

696 Integrated Climate Data Center (ICDC), CEN, and University of Hamburg, Hamburg, Germany: AMSR-E
697 Arctic lead area fraction, n.d.

698 Intergovernmental Panel On Climate Change: Climate Change 2021 – The Physical Science Basis: Working
699 Group I Contribution to the Sixth Assessment Report of the Intergovernmental Panel on Climate Change,
700 1st ed., Cambridge University Press, https://doi.org/10.1017/9781009157896, 2023.

701 Ioannidis, E., Law, K. S., Raut, J.-C., Marelle, L., Onishi, T., Kirpes, R. M., Upchurch, L. M., Tuch, T.,
702 Wiedensohler, A., Massling, A., Skov, H., Quinn, P. K., and Pratt, K. A.: Modelling wintertime sea-spray
703 aerosols under Arctic haze conditions, Atmospheric Chem. Phys., 23, 5641–5678,
704 https://doi.org/10.5194/acp-23-5641-2023, 2023.

705 Jaeglé, L., Quinn, P. K., Bates, T. S., Alexander, B., and Lin, J.-T.: Global distribution of sea salt aerosols:
706 new constraints from in situ and remote sensing observations, Atmospheric Chem. Phys., 11, 3137–3157,
707 https://doi.org/10.5194/acp-11-3137-2011, 2011.

708 Keller, C. A., Long, M. S., Yantosca, R. M., Da Silva, A. M., Pawson, S., and Jacob, D. J.: HEMCO v1.0: a
709 versatile, ESMF-compliant component for calculating emissions in atmospheric models, Geosci. Model
710 Dev., 7, 1409–1417, https://doi.org/10.5194/gmd-7-1409-2014, 2014.

711 Kirpes, R. M., Bonanno, D., May, N. W., Fraund, M., Barget, A. J., Moffet, R. C., Ault, A. P., and Pratt, K. A.:
712 Wintertime Arctic Sea Spray Aerosol Composition Controlled by Sea Ice Lead Microbiology, ACS Cent.
713 Sci., 5, 1760–1767, https://doi.org/10.1021/acscentsci.9b00541, 2019.

714 Leaitch, W. R., Russell, L. M., Liu, J., Kolonjari, F., Toom, D., Huang, L., Sharma, S., Chivulescu, A., Veber,
715 D., and Zhang, W.: Organic functional groups in the submicron aerosol at 82.5° N, 62.5° W from 2012 to
716 2014, Atmospheric Chem. Phys., 18, 3269–3287, https://doi.org/10.5194/acp-18-3269-2018, 2018.

717 Lin, H., Jacob, D. J., Lundgren, E. W., Sulprizio, M. P., Keller, C. A., Fritz, T. M., Eastham, S. D., Emmons, L.
718 K., Campbell, P. C., Baker, B., Saylor, R. D., and Montuoro, R.: Harmonized Emissions Component
719 (HEMCO) 3.0 as a versatile emissions component for atmospheric models: application in the GEOS-
720 Chem, NASA GEOS, WRF-GC, CESM2, NOAA GEFS-Aerosol, and NOAA UFS models, Geosci. Model Dev.,
721 14, 5487–5506, https://doi.org/10.5194/gmd-14-5487-2021, 2021.

722 Liu, H., Jacob, D. J., Bey, I., and Yantosca, R. M.: Constraints from ^{210}Pb and ^{7}Be on wet deposition and
723 transport in a global three-dimensional chemical tracer model driven by assimilated meteorological
724 fields, J. Geophys. Res. Atmospheres, 106, 12109–12128, https://doi.org/10.1029/2000JD900839, 2001.

Luo, G. and Yu, F.: Impact of Air Refreshing and Cloud Ice Uptake Limitations on Vertical Profiles and Wet Depositions of Nitrate, Ammonium, and Sulfate, Geophys. Res. Lett., 50, e2023GL104258, https://doi.org/10.1029/2023GL104258, 2023.

Luo, G., Yu, F., and Moch, J. M.: Further improvement of wet process treatments in GEOS-Chem v12.6.0: impact on global distributions of aerosols and aerosol precursors, Geosci. Model Dev., 13, 2879–2903, https://doi.org/10.5194/gmd-13-2879-2020, 2020.

May, N. W., Quinn, P. K., McNamara, S. M., and Pratt, K. A.: Multiyear study of the dependence of sea salt aerosol on wind speed and sea ice conditions in the coastal Arctic, J. Geophys. Res. Atmospheres, 121, 9208–9219, https://doi.org/10.1002/2016JD025273, 2016.

Monahan, E. C., Spiel, D. E., and Davidson, K. L.: A Model of Marine Aerosol Generation Via Whitecaps and Wave Disruption, in: Oceanic Whitecaps, vol. 2, edited by: Monahan, E. C. and Niocaill, G. M., Springer Netherlands, Dordrecht, 167–174, https://doi.org/10.1007/978-94-009-4668-2_16, 1986.

Nilsson, E. D., Rannik, Ü., Swietlicki, E., Leck, C., Aalto, P. P., Zhou, J., and Norman, M.: Turbulent aerosol fluxes over the Arctic Ocean: 2. Wind-driven sources from the sea, J. Geophys. Res. Atmospheres, 106, 32139–32154, https://doi.org/10.1029/2000JD900747, 2001.

Pierce, J. R. and Adams, P. J.: Global evaluation of CCN formation by direct emission of sea salt and growth of ultrafine sea salt, J. Geophys. Res. Atmospheres, 111, 2005JD006186, https://doi.org/10.1029/2005JD006186, 2006.

Pound, R. J., Sherwen, T., Helmig, D., Carpenter, L. J., and Evans, M. J.: Influences of oceanic ozone deposition on tropospheric photochemistry, Atmospheric Chem. Phys., 20, 4227–4239, https://doi.org/10.5194/acp-20-4227-2020, 2020.

Pratt, K. A., Custard, K. D., Shepson, P. B., Douglas, T. A., Pöhler, D., General, S., Zielcke, J., Simpson, W. R., Platt, U., Tanner, D. J., Gregory Huey, L., Carlsen, M., and Stirm, B. H.: Photochemical production of molecular bromine in Arctic surface snowpacks, Nat. Geosci., 6, 351–356, https://doi.org/10.1038/ngeo1779, 2013.

Quinn, P. K., Coffman, D. J., Kapustin, V. N., Bates, T. S., and Covert, D. S.: Aerosol optical properties in the marine boundary layer during the First Aerosol Characterization Experiment (ACE 1) and the underlying chemical and physical aerosol properties, J. Geophys. Res., 103, 16,547-16,563, 1998.

Quinn, P. K., Bates, T. S., Miller, T. L., Coffman, D. J., Johnson, J. E., Harris, J. M., Ogren, J. A., Forbes, G., Anderson, T. L., Covert, D. S., and Rood, M. J.: Surface submicron aerosol chemical composition: What fraction is not sulfate?, J. Geophys. Res. Atmospheres, 105, 6785–6805, https://doi.org/10.1029/1999JD901034, 2000.

Quinn, P. K., Miller, T. L., Bates, T. S., Ogren, J. A., Andrews, E., and Shaw, G. E.: A 3-year record of simultaneously measured aerosol chemical and optical properties at Barrow, Alaska, J. Geophys. Res. Atmospheres, 107, https://doi.org/10.1029/2001JD001248, 2002.

Radke, L. F., Hobbs, P. V., and Pinnons, J. E.: Observations of Cloud Condensation Nuclei, Sodium-Containing Particles, Ice Nuclei and the Light-Scattering Coefficient Near Barrow, Alaska, J. Appl. Meteor.

762 Climatol., 15, 982–995, https://doi.org/10.1175/1520-0450(1976)015%3C0982:OOCCNS%3E2.0.CO;2,
763 1976.

764 Rhodes, R. H., Yang, X., Wolff, E. W., McConnell, J. R., and Frey, M. M.: Sea ice as a source of sea salt
765 aerosol to Greenland ice cores: a model-based study, Atmospheric Chem. Phys., 17, 9417–9433,
766 https://doi.org/10.5194/acp-17-9417-2017, 2017.

767 Riley, J. P. and Chester, R.: Introduction to marine chemistry, Academic Press, London, New York, 465 pp.,
768 1971.

769 Röhrs, J. and Kaleschke, L.: An algorithm to detect sea ice leads by using AMSR-E passive microwave
770 imagery, The Cryosphere, 6, 343–352, https://doi.org/10.5194/tc-6-343-2012, 2012.

771 Roscoe, H. K., Brooks, B., Jackson, A. V., Smith, M. H., Walker, S. J., Obbard, R. W., and Wolff, E. W.: Frost
772 flowers in the laboratory: Growth, characteristics, aerosol, and the underlying sea ice, J. Geophys. Res.,
773 116, D12301, https://doi.org/10.1029/2010JD015144, 2011.

774 Salmi, T.: Measurement of Inorganics in air and particle phase at Pallas (Matorova) (3),
775 https://doi.org/10.48597/T6MX-CEKH, 2018.

776 Schmale, J., Zieger, P., and Ekman, A. M. L.: Aerosols in current and future Arctic climate, Nat. Clim.
777 Change, 11, 95–105, https://doi.org/10.1038/s41558-020-00969-5, 2021.

778 Scott, W. D. and Levin, Z.: Open Channels in Sea Ice (Leads) as Ion Sources, Science, 177, 425–426,
779 https://doi.org/10.1126/science.177.4047.425, 1972.

780 Screen, J. A. and Simmonds, I.: Declining summer snowfall in the Arctic: causes, impacts and feedbacks,
781 Clim. Dyn., 38, 2243–2256, https://doi.org/10.1007/s00382-011-1105-2, 2012.

782 Simpson, W. R., Alvarez-Aviles, L., Douglas, T. A., Sturm, M., and Domine, F.: Halogens in the coastal snow
783 pack near Barrow, Alaska: Evidence for active bromine air-snow chemistry during springtime, Geophys.
784 Res. Lett., 32, 2004GL021748, https://doi.org/10.1029/2004GL021748, 2005.

785 Simpson, W. R., Von Glasow, R., Riedel, K., Anderson, P., Ariya, P., Bottenheim, J., Burrows, J., Carpenter,
786 L. J., Frieß, U., Goodsite, M. E., Heard, D., Hutterli, M., Jacobi, H.-W., Kaleschke, L., Neff, B., Plane, J., Platt,
787 U., Richter, A., Roscoe, H., Sander, R., Shepson, P., Sodeau, J., Steffen, A., Wagner, T., and Wolff, E.:
788 Halogens and their role in polar boundary-layer ozone depletion, Atmospheric Chem. Phys., 7, 4375–
789 4418, https://doi.org/10.5194/acp-7-4375-2007, 2007.

790 Stramler, K., Del Genio, A. D., and Rossow, W. B.: Synoptically Driven Arctic Winter States, J. Clim., 24,
791 1747–1762, https://doi.org/10.1175/2010JCLI3817.1, 2011.

792 Stutz, J., Thomas, J. L., Hurlock, S. C., Schneider, M., Von Glasow, R., Piot, M., Gorham, K., Burkhart, J. F.,
793 Ziemba, L., Dibb, J. E., and Lefer, B. L.: Longpath DOAS observations of surface BrO at Summit, Greenland,
794 Atmospheric Chem. Phys., 11, 9899–9910, https://doi.org/10.5194/acp-11-9899-2011, 2011.

795 Sumata, H., De Steur, L., Divine, D. V., Granskog, M. A., and Gerland, S.: Regime shift in Arctic Ocean sea
796 ice thickness, Nature, 615, 443–449, https://doi.org/10.1038/s41586-022-05686-x, 2023.

797 Swanson, W. F., Holmes, C. D., Simpson, W. R., Confer, K., Marelle, L., Thomas, J. L., Jaeglé, L., Alexander,
798 B., Zhai, S., Chen, Q., Wang, X., and Sherwen, T.: Comparison of model and ground observations finds
799 snowpack and blowing snow aerosols both contribute to Arctic tropospheric reactive bromine,
800 Atmospheric Chem. Phys., 22, 14467–14488, https://doi.org/10.5194/acp-22-14467-2022, 2022.

801 Tan, I., Sotiropoulou, G., Taylor, P. C., Zamora, L., and Wendisch, M.: A Review of the Factors Influencing
802 Arctic Mixed-Phase Clouds: Progress and Outlook, in: Geophysical Monograph Series, edited by: Sullivan,
803 S. C. and Hoose, C., Wiley, 103–132, https://doi.org/10.1002/9781119700357.ch5, 2023.

804 Taylor, P. C., Boeke, R. C., Li, Y., and Thompson, D. W. J.: Arctic cloud annual cycle biases in climate
805 models, Atmospheric Chem. Phys., 19, 8759–8782, https://doi.org/10.5194/acp-19-8759-2019, 2019.

806 Vaughan, D., Comiso, J., Allison, I., Carrasco, J., Kaser, G., Kwok, R., Mote, P., Murray, T., Paul, F., Ren, J. F.,
807 Rignot, E., Solomina, O., Steffen, K., and Zhang, T.: Observations: Cryosphere, in: Climate Change 2013:
808 The Physical Science Basis, 317–382, 2013.

809 Villanueva, D., Possner, A., Neubauer, D., Gasparini, B., Lohmann, U., and Tesche, M.: Mixed-phase
810 regime cloud thinning could help restore sea ice, Environ. Res. Lett., 17, 114057,
811 https://doi.org/10.1088/1748-9326/aca16d, 2022.

812 Wang, Q., Jacob, D. J., Spackman, J. R., Perring, A. E., Schwarz, J. P., Moteki, N., Marais, E. A., Ge, C.,
813 Wang, J., and Barrett, S. R. H.: Global budget and radiative forcing of black carbon aerosol: Constraints
814 from pole-to-pole (HIPPO) observations across the Pacific, J. Geophys. Res. Atmospheres, 119, 195–206,
815 https://doi.org/10.1002/2013JD020824, 2014.

816 Wang, X., Jacob, D. J., Downs, W., Zhai, S., Zhu, L., Shah, V., Holmes, C. D., Sherwen, T., Alexander, B.,
817 Evans, M. J., Eastham, S. D., Neuman, J. A., Veres, P. R., Koenig, T. K., Volkamer, R., Huey, L. G., Bannan, T.
818 J., Percival, C. J., Lee, B. H., and Thornton, J. A.: Global tropospheric halogen (Cl, Br, I) chemistry and its
819 impact on oxidants, Atmospheric Chem. Phys., 21, 13973–13996, https://doi.org/10.5194/acp-21-13973-
820 2021, 2021.

821 Wang, Y., Jacob, D. J., and Logan, J. A.: Global simulation of tropospheric O_3-NO_x-hydrocarbon
822 chemistry: 3. Origin of tropospheric ozone and effects of nonmethane hydrocarbons, J. Geophys. Res.
823 Atmospheres, 103, 10757–10767, https://doi.org/10.1029/98JD00156, 1998.

824 Willis, M. D., Leaitch, W. R., and Abbatt, J. P. D.: Processes Controlling the Composition and Abundance of
825 Arctic Aerosol, Rev. Geophys., 56, 621–671, https://doi.org/10.1029/2018RG000602, 2018.

826 World Meteorological Organization (WMO): WMO/GAW aerosol measurement procedures, guidelines
827 and recommendations, WMO, Geneva, 2003.

828 Yang, X., Neděla, V., Runštuk, J., Ondrušková, G., Krausko, J., Vetráková, Ľ., and Heger, D.: Evaporating
829 brine from frost flowers with electron microscopy and implications for atmospheric chemistry and sea-
830 salt aerosol formation, Atmospheric Chem. Phys., 17, 6291–6303, https://doi.org/10.5194/acp-17-6291-
831 2017, 2017.

832 Zhang, L., Gong, S., Padro, J., and Barrie, L.: A size-segregated particle dry deposition scheme for an
833 atmospheric aerosol module, Atmos. Environ., 35, 549–560, 2001.

834